Measurement of the forward-backward asymmetry in $Z \to b\bar{b}$ and $Z \to c\bar{c}$ decays with leptons

A. Heister, S. Schael, R. Barate, I. de Bonis, D. Decamp, C. Goy, J P. Lees, E. Merle, M N. Minard, B. Pietrzyk, et al.

EUROPEAN ORGANIZATION FOR NUCLEAR RESEARCH (CERN)

CERN-EP/2001-097
December 21, 2001

Measurement of the Forward-Backward Asymmetry in $Z \to b\bar{b}$ and $Z \to c\bar{c}$ Decays with Leptons

The ALEPH Collaboration *)

Abstract

The sample of hadronic Z decays collected by the ALEPH detector at LEP in the years 1991-1995 is analysed in order to measure the forward-backward asymmetry in $Z \to b\bar{b}$ and $Z \to c\bar{c}$ events and the $B^0-\bar{B}^0$ average mixing parameter $\bar{\chi}$. Quark charges are tagged by the charges of electrons and muons produced in b and c semileptonic decays. Multivariate analyses are used to separate the event flavours and $b \to \ell/b \to c \to \ell$ processes. The b and c quark asymmetries are measured simultaneously; the average mixing parameter and the pole asymmetries are determined to be

$$\begin{aligned} \bar{\chi} &= 0.1196 \pm 0.0049\ (\text{stat.})\ ^{+0.0043}_{-0.0050}\ (\text{syst.}), \\ A_{FB}^{0,b} &= 0.0998 \pm 0.0040\ (\text{stat.})\ \pm 0.0017\ (\text{syst.}), \\ A_{FB}^{0,c} &= 0.0732 \pm 0.0053\ (\text{stat.})\ \pm 0.0037\ (\text{syst.}). \end{aligned}$$

These asymmetries, combined with the ALEPH measurements of the b asymmetry using inclusive b hadron decays and of the c asymmetry using reconstructed D mesons, correspond to a value of the effective electroweak mixing angle of $\sin^2\theta_W^{\text{eff}} = 0.23188 \pm 0.00046$.

Submitted to The European Physical Journal C

*) See next pages for the list of authors.

The ALEPH Collaboration

A. Heister, S. Schael

Physikalisches Institut das RWTH-Aachen, D-52056 Aachen, Germany

R. Barate, I. De Bonis, D. Decamp, C. Goy, J.-P. Lees, E. Merle, M.-N. Minard, B. Pietrzyk

Laboratoire de Physique des Particules (LAPP), IN^{2}P^3-CNRS, F-74019 Annecy-le-Vieux Cedex, France

G. Boix, S. Bravo, M.P. Casado, M. Chmeissani, J.M. Crespo, E. Fernandez, M. Fernandez-Bosman, Ll. Garrido,[15] E. Graugés, M. Martinez, G. Merino, R. Miquel,[27] Ll.M. Mir,[27] A. Pacheco, H. Ruiz

Institut de Física d'Altes Energies, Universitat Autònoma de Barcelona, E-08193 Bellaterra (Barcelona), Spain[7]

A. Colaleo, D. Creanza, M. de Palma, G. Iaselli, G. Maggi, M. Maggi, S. Nuzzo, A. Ranieri, G. Raso,[23] F. Ruggieri, G. Selvaggi, L. Silvestris, P. Tempesta, A. Tricomi,[3] G. Zito

Dipartimento di Fisica, INFN Sezione di Bari, I-70126 Bari, Italy

X. Huang, J. Lin, Q. Ouyang, T. Wang, Y. Xie, R. Xu, S. Xue, J. Zhang, L. Zhang, W. Zhao

Institute of High Energy Physics, Academia Sinica, Beijing, The People's Republic of China[8]

D. Abbaneo, P. Azzurri, O. Buchmüller,[25] M. Cattaneo, F. Cerutti, B. Clerbaux, H. Drevermann, R.W. Forty, M. Frank, F. Gianotti, T.C. Greening,[29] J.B. Hansen, J. Harvey, D.E. Hutchcroft, P. Janot, B. Jost, M. Kado,[27] P. Mato, A. Moutoussi, F. Ranjard, L. Rolandi, D. Schlatter, O. Schneider,[2] G. Sguazzoni, W. Tejessy, F. Teubert, A. Valassi, I. Videau, J. Ward

European Laboratory for Particle Physics (CERN), CH-1211 Geneva 23, Switzerland

F. Badaud, A. Falvard,[22] P. Gay, P. Henrard, J. Jousset, B. Michel, S. Monteil, J-C. Montret, D. Pallin, P. Perret

Laboratoire de Physique Corpusculaire, Université Blaise Pascal, IN^{2}P^3-CNRS, Clermont-Ferrand, F-63177 Aubière, France

J.D. Hansen, J.R. Hansen, P.H. Hansen, B.S. Nilsson, A. Wäänänen

Niels Bohr Institute, DK-2100 Copenhagen, Denmark[9]

A. Kyriakis, C. Markou, E. Simopoulou, A. Vayaki, K. Zachariadou

Nuclear Research Center Demokritos (NRCD), GR-15310 Attiki, Greece

A. Blondel,[12] G. Bonneaud, J.-C. Brient, A. Rougé, M. Rumpf, M. Swynghedauw, M. Verderi, H. Videau

Laboratoire de Physique Nucléaire et des Hautes Energies, Ecole Polytechnique, IN^{2}P^3-CNRS, F-91128 Palaiseau Cedex, France

V. Ciulli, E. Focardi, G. Parrini

Dipartimento di Fisica, Università di Firenze, INFN Sezione di Firenze, I-50125 Firenze, Italy

A. Antonelli, M. Antonelli, G. Bencivenni, G. Bologna,[4] F. Bossi, P. Campana, G. Capon, V. Chiarella, P. Laurelli, G. Mannocchi,[5] F. Murtas, G.P. Murtas, L. Passalacqua, M. Pepe-Altarelli,[24]

Laboratori Nazionali dell'INFN (LNF-INFN), I-00044 Frascati, Italy

A. Halley, J.G. Lynch, P. Negus, V. O'Shea, C. Raine,[4] A.S. Thompson

Department of Physics and Astronomy, University of Glasgow, Glasgow G12 8QQ,United Kingdom[10]

S. Wasserbaech

Department of Physics, Haverford College, Haverford, PA 19041-1392, U.S.A.

R. Cavanaugh, S. Dhamotharan, C. Geweniger, P. Hanke, G. Hansper, V. Hepp, E.E. Kluge, A. Putzer, J. Sommer, H. Stenzel, K. Tittel, S. Werner,[19] M. Wunsch[19]

Kirchhoff-Institut für Physik, Universität Heidelberg, D-69120 Heidelberg, Germany[16]

R. Beuselinck, D.M. Binnie, W. Cameron, P.J. Dornan, M. Girone,[1] N. Marinelli, J.K. Sedgbeer,

J.C. Thompson[14]

Department of Physics, Imperial College, London SW7 2BZ, United Kingdom[10]

V.M. Ghete, P. Girtler, E. Kneringer, D. Kuhn, G. Rudolph

Institut für Experimentalphysik, Universität Innsbruck, A-6020 Innsbruck, Austria[18]

E. Bouhova-Thacker, C.K. Bowdery, A.J. Finch, F. Foster, G. Hughes, R.W.L. Jones, M.R. Pearson, N.A. Robertson

Department of Physics, University of Lancaster, Lancaster LA1 4YB, United Kingdom[10]

K. Jakobs, K. Kleinknecht, G. Quast,[6] B. Renk, H.-G. Sander, H. Wachsmuth, C. Zeitnitz

Institut für Physik, Universität Mainz, D-55099 Mainz, Germany[16]

A. Bonissent, J. Carr, P. Coyle, O. Leroy, P. Payre, D. Rousseau, M. Talby

Centre de Physique des Particules, Université de la Méditerranée, IN^{2}P^3-CNRS, F-13288 Marseille, France

F. Ragusa

Dipartimento di Fisica, Università di Milano e INFN Sezione di Milano, I-20133 Milano, Italy

A. David, H. Dietl, G. Ganis,[26] K. Hüttmann, G. Lütjens, C. Mannert, W. Männer, H.-G. Moser, R. Settles, W. Wiedenmann, G. Wolf

Max-Planck-Institut für Physik, Werner-Heisenberg-Institut, D-80805 München, Germany[16]

J. Boucrot, O. Callot, M. Davier, L. Duflot, J.-F. Grivaz, Ph. Heusse, A. Jacholkowska, J. Lefrançois, J.-J. Veillet, C. Yuan

Laboratoire de l'Accélérateur Linéaire, Université de Paris-Sud, IN^{2}P^3-CNRS, F-91898 Orsay Cedex, France

G. Bagliesi, T. Boccali, L. Foà, A. Giammanco, A. Giassi, F. Ligabue, A. Messineo, F. Palla, G. Sanguinetti, A. Sciabà, R. Tenchini,[1] A. Venturi,[1] P.G. Verdini

Dipartimento di Fisica dell'Università, INFN Sezione di Pisa, e Scuola Normale Superiore, I-56010 Pisa, Italy

G.A. Blair, G. Cowan, M.G. Green, T. Medcalf, A. Misiejuk, J.A. Strong, P. Teixeira-Dias, J.H. von Wimmersperg-Toeller

Department of Physics, Royal Holloway & Bedford New College, University of London, Egham, Surrey TW20 OEX, United Kingdom[10]

R.W. Clifft, T.R. Edgecock, P.R. Norton, I.R. Tomalin

Particle Physics Dept., Rutherford Appleton Laboratory, Chilton, Didcot, Oxon OX11 OQX, United Kingdom[10]

B. Bloch-Devaux, P. Colas, S. Emery, W. Kozanecki, E. Lançon, M.-C. Lemaire, E. Locci, P. Perez, J. Rander, J.-F. Renardy, A. Roussarie, J.-P. Schuller, J. Schwindling, A. Trabelsi,[21] B. Vallage

CEA, DAPNIA/Service de Physique des Particules, CE-Saclay, F-91191 Gif-sur-Yvette Cedex, France[17]

N. Konstantinidis, A.M. Litke, G. Taylor

Institute for Particle Physics, University of California at Santa Cruz, Santa Cruz, CA 95064, USA[13]

C.N. Booth, S. Cartwright, F. Combley,[4] M. Lehto, L.F. Thompson

Department of Physics, University of Sheffield, Sheffield S3 7RH, United Kingdom[10]

K. Affholderbach,[28] A. Böhrer, S. Brandt, C. Grupen, A. Ngac, G. Prange, U. Sieler

Fachbereich Physik, Universität Siegen, D-57068 Siegen, Germany[16]

G. Giannini

Dipartimento di Fisica, Università di Trieste e INFN Sezione di Trieste, I-34127 Trieste, Italy

J. Rothberg

Experimental Elementary Particle Physics, University of Washington, Seattle, WA 98195 U.S.A.

S.R. Armstrong, K. Berkelman, K. Cranmer, D.P.S. Ferguson, Y. Gao,[20] S. González, O.J. Hayes, H. Hu, S. Jin, J. Kile, P.A. McNamara III, J. Nielsen, Y.B. Pan, J.H. von Wimmersperg-Toeller, W. Wiedenmann, J. Wu, Sau Lan Wu, X. Wu, G. Zobernig

Department of Physics, University of Wisconsin, Madison, WI 53706, USA[11]

G. Dissertori

Institute for Particle Physics, ETH Hönggerberg, 8093 Zürich, Switzerland.

[1]Also at CERN, 1211 Geneva 23, Switzerland.
[2]Now at Université de Lausanne, 1015 Lausanne, Switzerland.
[3]Also at Dipartimento di Fisica di Catania and INFN Sezione di Catania, 95129 Catania, Italy.
[4]Deceased.
[5]Also Istituto di Cosmo-Geofisica del C.N.R., Torino, Italy.
[6]Now at Institut für Experimentelle Kernphysik, Universität Karlsruhe, 76128 Karlsruhe, Germany.
[7]Supported by CICYT, Spain.
[8]Supported by the National Science Foundation of China.
[9]Supported by the Danish Natural Science Research Council.
[10]Supported by the UK Particle Physics and Astronomy Research Council.
[11]Supported by the US Department of Energy, grant DE-FG0295-ER40896.
[12]Now at Departement de Physique Corpusculaire, Université de Genève, 1211 Genève 4, Switzerland.
[13]Supported by the US Department of Energy, grant DE-FG03-92ER40689.
[14]Also at Rutherford Appleton Laboratory, Chilton, Didcot, UK.
[15]Permanent address: Universitat de Barcelona, 08208 Barcelona, Spain.
[16]Supported by the Bundesministerium für Bildung, Wissenschaft, Forschung und Technologie, Germany.
[17]Supported by the Direction des Sciences de la Matière, C.E.A.
[18]Supported by the Austrian Ministry for Science and Transport.
[19]Now at SAP AG, 69185 Walldorf, Germany.
[20]Also at Department of Physics, Tsinghua University, Beijing, The People's Republic of China.
[21]Now at Département de Physique, Faculté des Sciences de Tunis, 1060 Le Belvédère, Tunisia.
[22]Now at Groupe d'Astroparticules de Montpellier, Université de Montpellier II, 34095, Montpellier, France
[23]Also at Dipartimento di Fisica e Tecnologie Relative, Università di Palermo, Palermo, Italy.
[24]Now at CERN, 1211 Geneva 23, Switzerland.
[25]Now at SLAC, Stanford, CA 94309, U.S.A.
[26]Now at INFN Sezione di Roma II, Dipartimento di Fisica, Universitá di Roma Tor Vergata, 00133 Roma, Italy.
[27]Now at LBNL, Berkeley, CA 94720, U.S.A.
[28]Now at Skyguide, Swissair Navigation Services, Geneva, Switzerland.
[29]Now at Honeywell, Phoenix AZ, U.S.A.

1 Introduction

The forward-backward asymmetry of the quarks in $Z \to q\bar{q}$ decays provides a precise measurement of the electroweak mixing angle $\sin^2\theta^{\rm eff}_{\rm W}$ and thus an important test of the Standard Model. This asymmetry arises from the interference between the vector and axial-vector couplings of the Z to the quarks, and as these are different for up- and down-type quarks, flavour separation is essential. Of the five flavours produced at LEP only samples of b and c quarks can be isolated with adequate purity and efficiency; the b asymmetry is the observable with the highest sensitivity to $\sin^2\theta^{\rm eff}_{\rm W}$ at LEP. This paper gives measurements of these asymmetries using the charge of the electrons and muons from semileptonic decays to identify the quark charge.

With respect to the previous analysis [1], the main advantage of the present technique is related to the capability of measuring both the b and c asymmetries, which, when interpreted in terms of $\sin^2\theta^{\rm eff}_{\rm W}$, improves the accuracy of the measurement by 30%. The present analysis takes advantage of both an upgraded track reconstruction and improved particle identification in the recently reprocessed 3.9 million hadronic Z decays recorded at LEP1.

For the b asymmetry, $\rm B^0{-}\bar{B}^0$ mixing and cascade decays lead to the incorrect charge tagging. The average mixing parameter is measured in the same data sample by analysing events with two leptons. Kinematical and topological properties are used to separate direct from cascade decays, thus reducing the dilution of the observed asymmetry. The asymmetries $\rm A^b_{FB}$ and $\rm A^c_{FB}$ are then simultaneously measured from a fit to the polar angle distribution of the thrust axis for events containing at least one identified lepton candidate. The results are combined with the ALEPH measurements of the b asymmetry using inclusive b hadron decays and of the c asymmetry using reconstructed D mesons [2, 3].

2 The ALEPH detector and the event selection

The analysis is based on 3.9 million hadronic Z decays collected with the ALEPH detector from 1991 to 1995. A detailed description of the detector and its performance is given elsewhere [4, 5]. A brief overview will be given here, together with some basic information on lepton identification. Charged particles are tracked in a two-layer silicon vertex detector (VDET) with double-sided readout (r-ϕ and z), surrounded by a cylindrical drift chamber and a large time projection chamber (TPC), together measuring up to 33 three-dimensional coordinates. These detectors are immersed in a 1.5 T axial magnetic field, providing a resolution on the transverse momentum relative to the beam axis of $\Delta p_{\rm T}/p_{\rm T} = (6 \times 10^{-4})\, p_{\rm T} \oplus 0.005$ ($p_{\rm T}$ in GeV/c) and a three-dimensional impact parameter resolution of $25\,\mu{\rm m} + 95\,\mu{\rm m}/p$ (p in GeV/c) for tracks having two VDET hits. The TPC also allows particle identification through the measurement of the specific ionization ($\mathrm{d}E/\mathrm{d}x$). The electrons are separated from the other charged particles by more than three standard deviations up to a momentum of 8 GeV/c. A finely segmented electromagnetic calorimeter of lead/wire-chamber sandwich construction surrounds the TPC. Its energy resolution is $\Delta E/E = 0.18/\sqrt{E} \oplus 0.009$ (E in GeV). Electrons are identified by the longitudinal and transverse characteristics of their shower in the ECAL, together with the $\mathrm{d}E/\mathrm{d}x$ information. The iron return yoke of the magnet is instrumented with streamer tubes to form the hadron calorimeter, which is surrounded by two additional double layers of streamer tubes for muon identification.

The sample of $Z \to q\bar{q}$ events considered in the analysis is selected as described in [6], using all the data collected by ALEPH in the years 1991-1995. Within this sample, electrons and muons are identified according to the procedure described in [7]. However, in order to increase the statistics of the sample, the momentum acceptance cut is relaxed to $p > 2$ GeV/c for electron candidates and $p > 2.5$ GeV/c for muon candidates.

During 1998, the LEP1 data were reprocessed using a refined version of the reconstruction program, obtaining increased efficiency and precision in track reconstruction and enhanced performance in particle identification. The improvements most relevant for the analysis discussed

in this paper are the increase in the electron identification efficiency, no longer dependent on the track isolation, and the reduction in the background to muon identification [8]. The $\mathrm{d}E/\mathrm{d}x$ is also used in the muon identification procedure, removing about half of the misidentified kaons with only a small effect on the prompt muon efficiency [9].

Jets are found using the JADE algorithm [10]; the cut on the jet invariant mass is set at $M_{\mathrm{jet}} = 6$ GeV/c^2. The lepton transverse momentum, $p_\perp$, is calculated with respect to the jet axis after removing the lepton itself, in order to achieve the best discrimination of $b \to \ell$ decays from the other lepton sources [7].

The asymmetry analysis is event based. Hadronic events with at least one lepton candidate are selected. If more than one lepton candidate is found, the one with the highest $p_\perp$ is retained, as it has higher probability to bring the correct information on the quark charge. For each event, the thrust axis, taken as the experimental estimator of the quark initial direction, is measured from all reconstructed charged and neutral particles [4]. The cosine of the polar angle of the thrust axis must be less than 0.9 to reject events with substantial losses in the beam pipe. The event is divided into two hemispheres using the plane perpendicular to the thrust axis. The b (c) quark hemisphere is then taken to be the one containing the jet with the lepton, if the lepton charge is negative (positive), the opposite hemisphere otherwise. Events are grouped according to the centre-of-mass energy and at each energy point a simultaneous measurement of $\mathrm{A}^{\mathrm{b}}_{\mathrm{FB}}$ and $\mathrm{A}^{\mathrm{c}}_{\mathrm{FB}}$ is performed. A total of 504,914 events are selected. The measurement of the average time-integrated mixing in b events is based upon events with at least one lepton per hemisphere, fulfilling the above selection procedure. A total of 296,911 dilepton events are selected.

3 The flavour separation

Two discriminating multivariate quantities, N_{b} and N_{uds}, designed to tag respectively b and uds events are built using a single neural network with two outputs. The best flavour separation is obtained with the following set of variables:

- P_{E}, a b tagging variable based on the impact parameter significance of charge particle tracks [11];
- p, the lepton momentum;
- $p_\perp$, the lepton transverse momentum;
- $\not\!\!E$, the missing energy of the event;
- $\sum_i p^2_{\perp i}$, where $p_{\perp i}$ is the transverse momentum of the i^{th} track of the most energetic jet in the event. The i^{th} track is included in the computation of the jet axis;
- $\Delta\chi^2_{\mathrm{V}}$, the difference between the χ^2 of the fit with all tracks assigned to the primary vertex and the χ^2 of the fit with inclusively reconstructed secondary vertices [12];
- p_{fast}, the momentum of the highest momentum particle of the event;
- $p^2_{\perp\pi_{\mathrm{s}}}$, the transverse momentum squared of a particle (if any) with kinematics matching the π_{s} hypothesis [13], where π_{s} indicates the pion produced in the decay $\mathrm{D}^* \to \mathrm{D}\pi_{\mathrm{s}}$. If more than one particle is selected, the best candidate is chosen.

The most discriminating among these variables are plotted in Fig. 1. The long lifetime of b-hadrons (which is exploited in P_{E} and $\Delta\chi^2_{\mathrm{V}}$), the high mass of the b quarks (entering through $\sum_i p^2_{\perp i}$) and the semileptonic decay kinematical properties (p, $p_\perp$ and $\not\!\!E$) provide valuable information for flavour separation, with charm events having intermediate properties between b and light quark events. The variables p_{fast} and $p^2_{\perp\pi_{\mathrm{s}}}$ yield further separation between charm

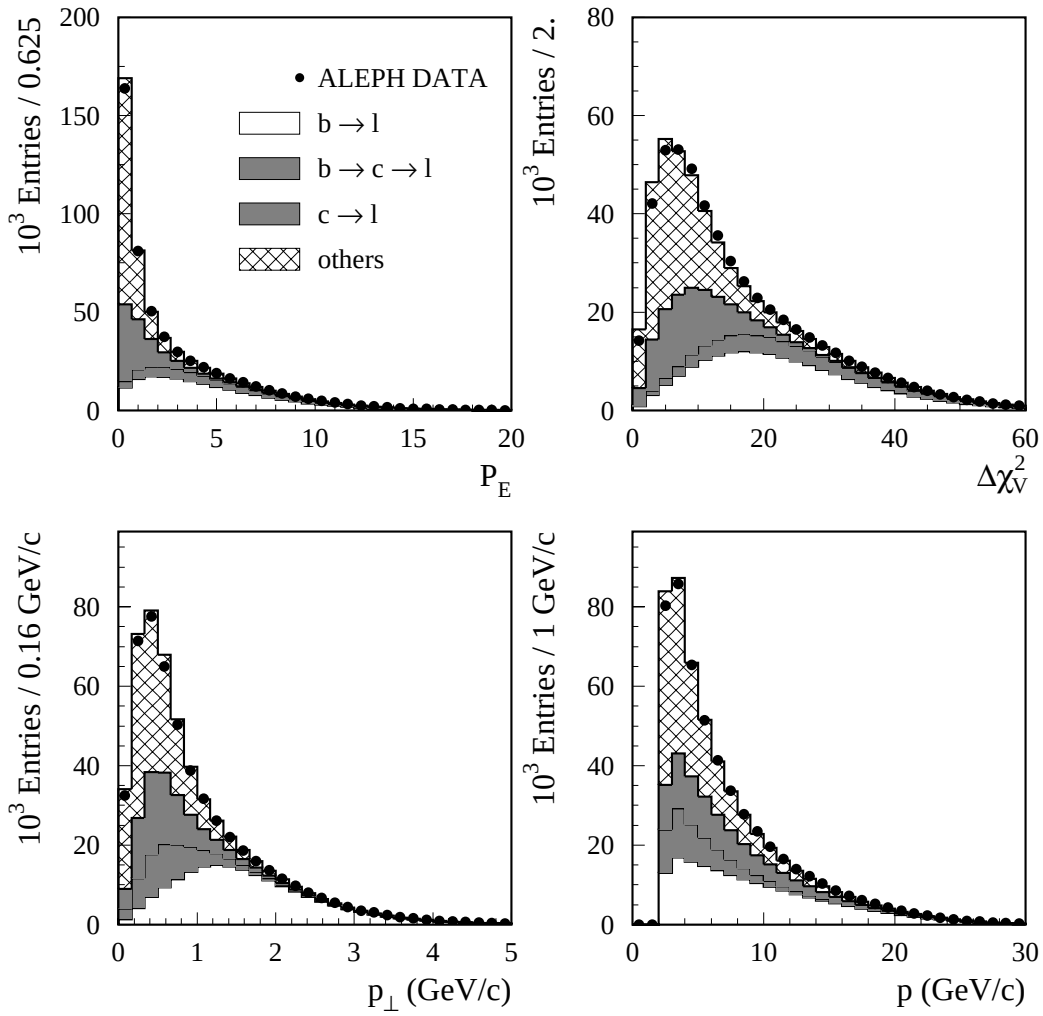

Figure 1: Distributions of the most discriminating input variables used in the construction of the combined neural network variables N_{b} and N_{uds}.

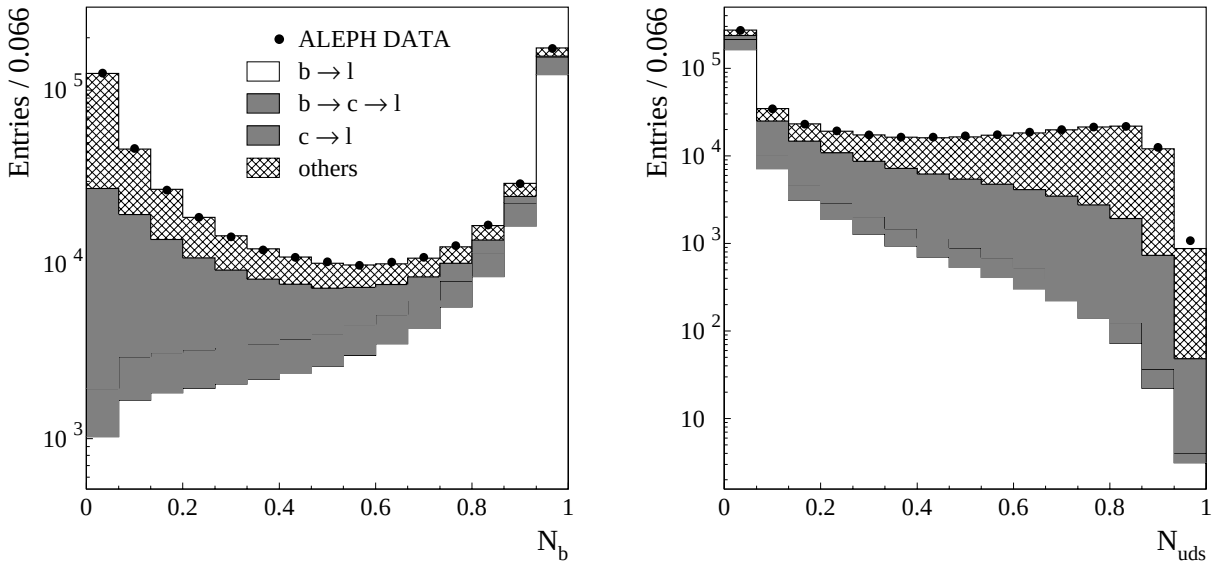

Figure 2: The distribution of the discriminating variables N_{b} and N_{uds}.

and light quark events; the highest momentum particle of the event has on average a harder spectrum in light quark events due to the lower particle multiplicity and the pion from the $\mathrm{D}^* \to \mathrm{D}\pi_{\mathrm{s}}$ decay tends to be collinear with the jet axis, especially in charm events where D^* are produced with a harder spectrum compared to b events.

All these variables are used simultaneously in the neural network to form the two discriminating variables N_{b} and N_{uds} plotted in Fig. 2.

Since the discriminating power of lifetime variables based on VDET information (P_{E} and $\Delta\chi^2_{\mathrm{V}}$) decreases at large polar angles, the variable $\cos\theta_{\mathrm{thrust}}$ is used in the neural network, ensuring an adequate assignment of the weights according to the angle.

4 The separation of the $\mathrm{b} \to \ell$ and $\mathrm{b} \to \mathrm{c} \to \ell$ processes

Assuming a perfect flavour separation, the statistical uncertainty on $\mathrm{A}^{\mathrm{b}}_{\mathrm{FB}}$ is proportional, to a first approximation, to the inverse of the difference $(f_{\mathrm{b}\to\ell} - f_{\mathrm{b}\to\mathrm{c}\to\ell})$, where $f_{\mathrm{b}\to\mathrm{X}}$ is the fraction of $\mathrm{b} \to \mathrm{X}$ events in the sample. It is therefore important to achieve the best possible separation between these two processes. In the previously published ALEPH analyses [1, 14], only the kinematical properties of the lepton were used in that respect. The separation is improved here by considering the properties of the b hadron jet to which the lepton candidate belongs, exploiting the different jet topologies of $\mathrm{X_b} \to \ell\nu\mathrm{X_c}$ and $\mathrm{X_b} \to \mathrm{W}^*\mathrm{X_c}(\mathrm{X_c} \to \ell\nu\mathrm{X})$ decays, where $\mathrm{X_b}(\mathrm{X_c})$ indicates any b(c) hadron. Due to the fact that these properties are linked to the weakly decaying b-hadron, a different approach of clustering, generally used at the hadron colliders and first developed at LEP by OPAL [15] is chosen to measure the lepton jet properties. The procedure, based on a geometrical association of the tracks, is governed by two cut parameters related to the energy ($\mathcal{E} = 5$ GeV) and the opening angle ($\mathcal{R} = 0.4$ rad) of the jet. This clustering approach leads to a typical 10% improvement both in terms of the b tracks selection efficiency and of the rejection of fragmentation tracks, with respect to the JADE algorithm.

The boost of the b hadron tends to dilute some of the topological differences between the $\mathrm{b} \to \ell$ and $\mathrm{b} \to \mathrm{c} \to \ell$ decays discussed above. It is therefore useful to study the separation by boosting the particles of the jet to the $(\ell\mathrm{X_c})$ rest frame, without considering the neutrino. In this frame two hemispheres are defined according to the plane perpendicular to the lepton

direction. Four variables are then constructed for $b \to \ell$ / $b \to c \to \ell$ separation:

- $E_{\rm CM1}$ is defined as the sum of energies of the tracks belonging to the lepton hemisphere, excluding the lepton itself. The c hadron and the lepton issued from the decay $X_b \to X_c \ell \nu$ are by construction produced back to back in the (ℓX_c) frame. On the contrary, the lepton originating from the cascade decay $X_b \to W^* X_c (X_c \to X \ell \nu)$ should be found close in phase space with the X system. Low values of $E_{\rm CM1}$ are therefore a signature for $b \to \ell$ decays.
- $P_{\rm lt} = \frac{|P_+ - P_-|}{P_+ + P_-}$ where P_+ (P_-) is the sum of the parallel (antiparallel) momenta of the jet tracks (lepton excluded) with respect to the lepton direction. $P_{\rm lt}$ exploits the fact that in most of the $b \to c \to \ell$ decays hadronization occurs in both (ℓX_c) hemispheres (because of the c quark and the W decay products). A high value of $P_{\rm lt}$ is thus more likely for the $b \to \ell$ events.
- $E_{\rm jet} = \sum_i E_i$, where E_i is the energy of the $i^{\rm th}$ track of the jet in the (ℓX_c) frame.
- $E_{\rm lCM}$, the energy of the lepton candidate in the (ℓX_c) frame.

These four variables are combined using a neural network (to form the quantity $N_{\rm bl}$), together with the three variables based on the kinematical properties of the lepton, which were used also for the flavour separation:

- p, the lepton momentum,
- $p_\perp$, the lepton transverse momentum,
- $\not{E}$, the missing energy of the event.

Fig. 3 displays the distributions of the four most discriminating variables ($p_\perp$, $E_{\rm lCM}$, $P_{\rm lt}$ and $E_{\rm CM1}$) in a sample of data and simulated events enriched in b events ($N_{\rm b} > 0.96$); Fig. 4 shows the resulting distribution of $N_{\rm bl}$ in the same sample. In these figures simulated events are reweighted to reproduce the lepton energy spectrum in the b hadron rest frame given by the ISGW model [16] (Section 7.2). The combined variable $N_{\rm bl}$ provides a substantially enhanced discriminating power compared to the lepton transverse momentum, which translates to a reduction of the statistical uncertainty of $A_{\rm FB}^{\rm b}$ by about 10%.

5 The fitting method

The asymmetries are extracted from a binned maximum likelihood fit to the distribution of events in the space $(N_{\rm b}, N_{\rm uds}, N_{\rm bl}, x)$, where x is the signed quantity $-Q\cos\theta_{\rm thrust}$ and Q the electric charge of the lepton candidate. The total log-likelihood is

$$-\ln\mathcal{L} = -\sum_{ijkl} n_{ijkl} \ln f_{ijkl} \ , \tag{1}$$

where n_{ijkl} is the number of lepton candidates in the data sample in the bin (i,j,k,l) of $(N_{\rm b}, N_{\rm uds}, N_{\rm bl}, x)$ and f_{ijkl} is the expected number of events. The binning is chosen to ensure a comparable occupancy of the bins; each is filled by approximately 500 data events. Fig. 5 shows the binning in the plane $(N_{\rm b}, N_{\rm uds})$. The variable $N_{\rm bl}$ is only used in the region defined by the first bin of $N_{\rm uds}$, which contains most of the b events. The distribution of the different processes in the $(N_{\rm b}, N_{\rm bl})$ plane is shown in Fig. 6. Altogether the space $(N_{\rm b}, N_{\rm uds}, N_{\rm bl})$ is divided in 70 bins and the angular range is split in 20 equal-sized bins.

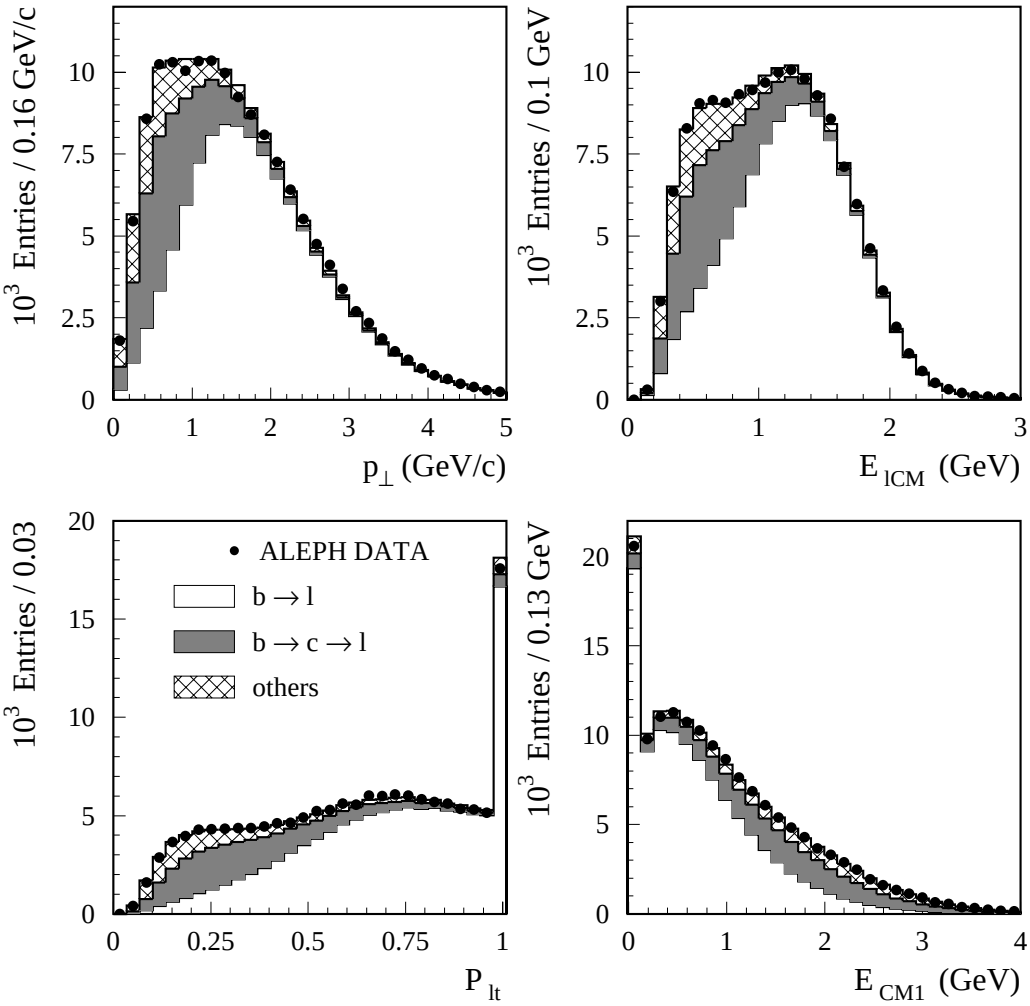

Figure 3: Distributions of four discriminating variables used for b $\to \ell$ tagging in data and simulation, for events satisfying a tight b tagging cut $N_b > 0.96$. In the simulation, for b $\to \ell$ decays, the lepton energy in the b hadron rest frame is reweighted according to the ISGW model.

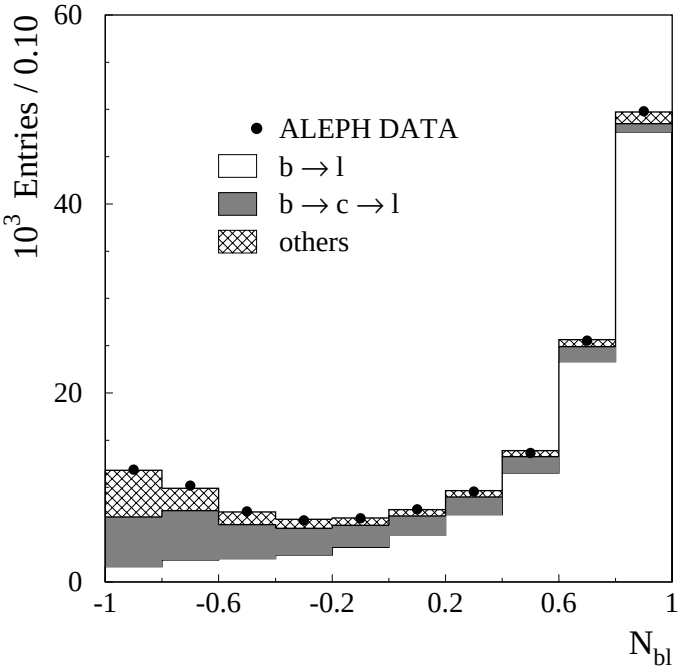

Figure 4: The distribution of the combined variable $N_{\rm bl}$ in an enriched sample of b events ($N_{\rm b} > 0.96$). In the simulation, for $\mathrm{b} \to \ell$ decays, the lepton energy in the b hadron rest frame is reweighted according to the ISGW model.

The expected number of events f_{ijkl} normalised to unity is given by

$$
\begin{aligned}
f_{ijkl} &= (F^{\rm rs}_{\ell,{\rm b}})_{ijkl} \int_l [1 + x^2 + \frac{8}{3} {\rm A}^{\rm b}_{\rm FB} (1 - 2\overline{\chi}_{ijkl})\, x] {\rm d}x \\
&+ (F^{\rm ws}_{\ell,{\rm b}})_{ijkl} \int_l [1 + x^2 - \frac{8}{3} {\rm A}^{\rm b}_{\rm FB} (1 - 2\overline{\chi}_{ijkl})\, x] {\rm d}x \\
&+ (F^{\rm asym}_{\rm bkg,b})_{ijkl} \int_l [1 + x^2 + \frac{8}{3} {\rm A}^{\rm b}_{\rm FB} (1 - 2\overline{\chi}_{ijkl})(2\eta^{\rm b}_{ijk} - 1)\, x] {\rm d}x \\
&+ (F_{\ell,{\rm c}})_{ijkl} \int_l (1 + x^2 - \frac{8}{3} {\rm A}^{\rm c}_{\rm FB}\, x) {\rm d}x \\
&+ (F^{\rm asym}_{\rm c\to bkg})_{ijkl} \int_l [1 + x^2 - \frac{8}{3} {\rm A}^{\rm c}_{\rm FB} (2\eta^{\rm c}_{ijk} - 1)\, x] {\rm d}x \\
&+ (F^{\rm asym}_{\rm s\to bkg})_{ijkl} \int_l [1 + x^2 + \frac{8}{3} {\rm A}^{\rm s}_{\rm FB} (2\eta^{\rm s}_{ijk} - 1)\, x] {\rm d}x \\
&+ (F^{\rm asym}_{\rm d\to bkg})_{ijkl} \int_l [1 + x^2 + \frac{8}{3} {\rm A}^{\rm d}_{\rm FB} (2\eta^{\rm d}_{ijk} - 1)\, x] {\rm d}x \\
&+ (F^{\rm asym}_{\rm u\to bkg})_{ijkl} \int_l [1 + x^2 - \frac{8}{3} {\rm A}^{\rm u}_{\rm FB} (2\eta^{\rm u}_{ijk} - 1)\, x] {\rm d}x \\
&+ (F^{\rm sym}_{\rm bkg})_{ijkl} \int_l (1 + x^2) {\rm d}x, \qquad (2)
\end{aligned}
$$

where all semileptonic b decays are divided into *right sign* (rs) and *wrong sign* (ws) decays, according to whether the lepton charge is the same or opposite sign to that of the parent b quark (after any mixing has occurred). The fitted quantities are $\mathrm{A}^{\rm b}_{\rm FB}$ and $\mathrm{A}^{\rm c}_{\rm FB}$. All processes contributing to the lepton candidate samples are classified depending upon their contribution to the forward-backward asymmetry. The fractions $F_{\rm process}$ are determined from simulated events.

The observed asymmetry in b events is diluted by B^0–$\bar{\mathrm{B}}^0$ oscillations. The average mixing

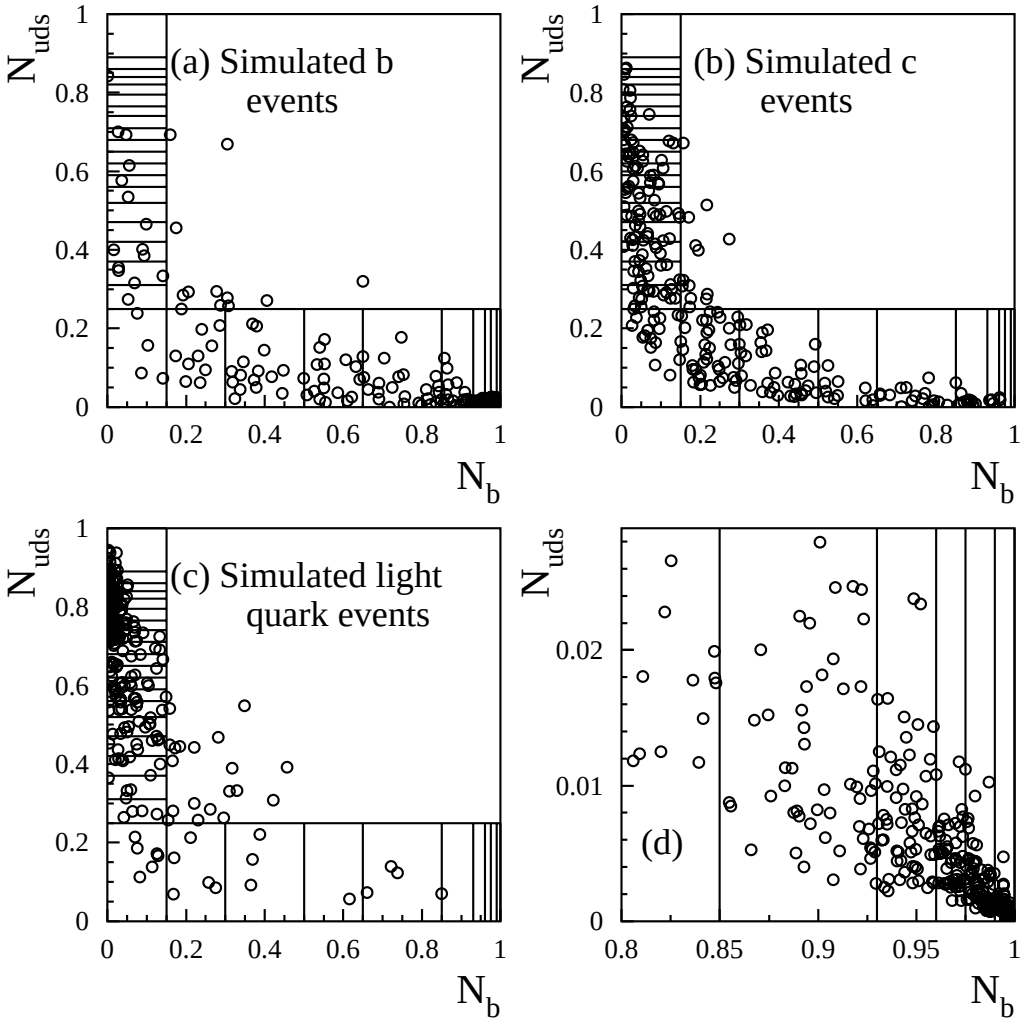

Figure 5: Distribution of simulated events in the $(N_{\rm b}, N_{\rm uds})$ plane. Plots (a) (b) and (c) show the distributions of 1000 b, c and light quark events, respectively. The region defined by $N_{\rm uds} < 0.25$ is divided in 10 intervals of $N_{\rm b}$; each of these bins is then further split in 5 equal-sized bins of $N_{\rm bl}$, to discriminate direct decays from cascade decays. The region $N_{\rm b} < 0.15$ is divided in 20 intervals of $N_{\rm uds}$, to improve the separation between charm and light quark events. The rest of the plane is contained in a single bin as it is populated by little statistics. Plot (d) is a zoom of the bottom-right corner of plot (a).

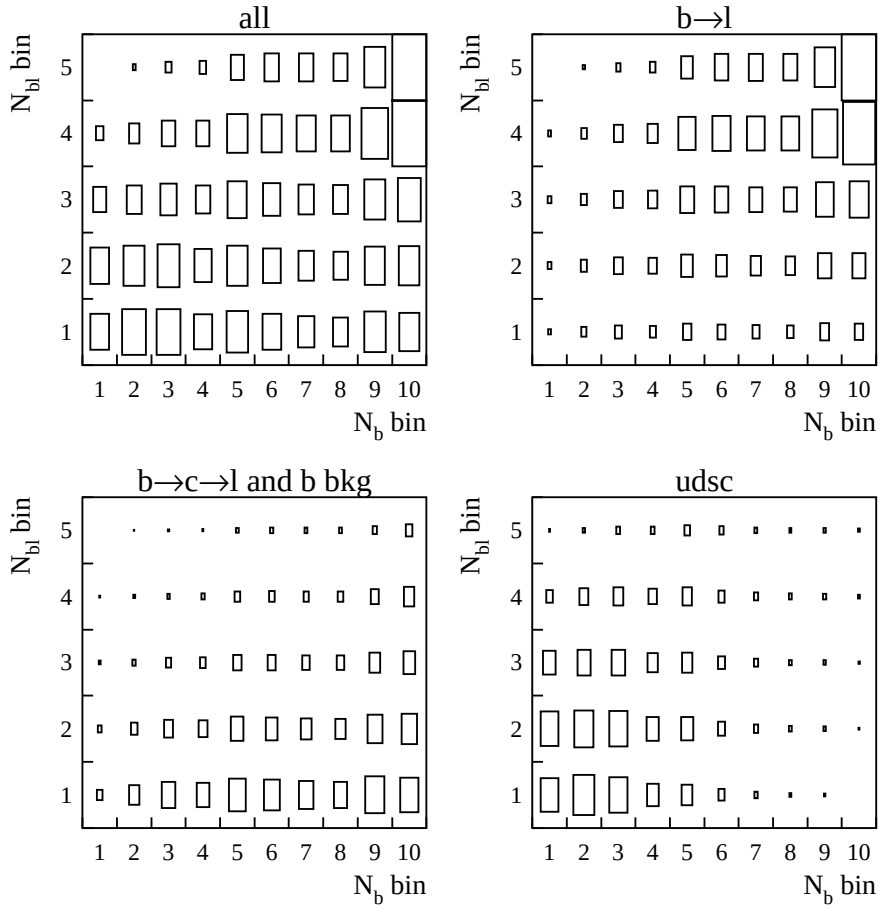

Figure 6: Distribution in bins of $(N_{\rm b}, N_{\rm bl})$ of simulated events with $N_{\rm uds} < 0.25$.

parameter $\bar{\chi}$ can be written as

$$\bar{\chi} = f_{\rm B^0_d}\chi_{\rm d}{\rm BR}({\rm B^0_d} \to \ell)/{\rm BR}({\rm b} \to \ell) + f_{\rm B^0_s}\chi_{\rm s}{\rm BR}({\rm B^0_s} \to \ell)/{\rm BR}({\rm b} \to \ell)\ ,$$

where $f_{\rm B^0_q}$ is the production fraction of the neutral B meson of flavour q and $\chi_{\rm q}$ is the ${\rm B^0_q}$–$\bar{\rm B}^0_{\rm q}$ integrated mixing probability. In the analysis, events populating the different $N_{\rm b}$ and $N_{\rm uds}$ bins have different proper time distributions due to the use of lifetime-based variables for the flavour separation. Therefore an effective mixing rate $\bar{\chi}_{ijkl}$ has to be evaluated bin by bin with the simulation, and folded in the extraction of the asymmetries. Simulated events are reweighted to reproduce the measured value of the average time-integrated mixing rate (Section 6).

Some fake leptons, such as muons from K decay following the b → c → s chain, do carry information about the original quark charge as discussed in greater detail in [1] and therefore the background is split into symmetric and asymmetric contributions. The latter is quantified by a parameter η which gives the probability that a background lepton candidate has the same charge sign as the decaying quark. For a given flavour, η depends upon the momentum and the background particle, as illustrated in Fig. 7.

6 Measurement of the average time-integrated mixing

The average time-integrated mixing rate $\bar{\chi}$, defined in Section 5, is measured using events with one lepton candidate per hemisphere, with the selection described in Section 2 applied to both

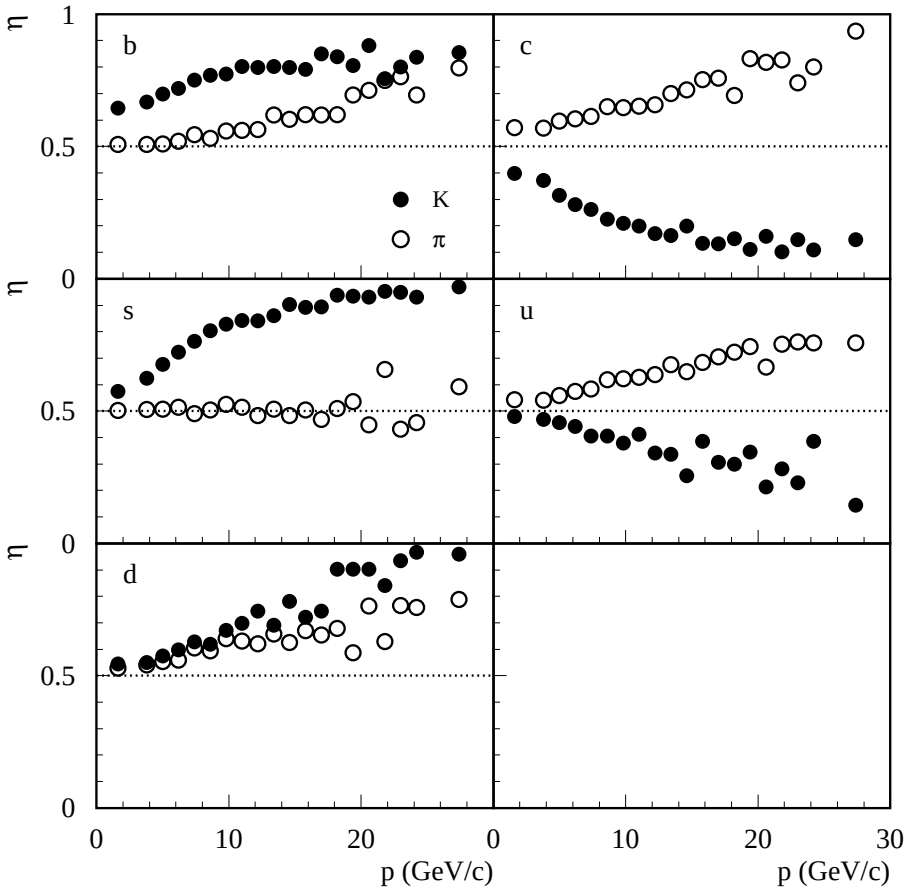

Figure 7: Distribution of the probability that a background lepton candidate has the same electric charge sign as the primary quark, as a function of its momentum, for the five quark flavours. Charged kaons and pions are represented with black and white dots respectively.

leptons. Background from Z decays to light quarks is further rejected with the cut $N_{\rm uds} < 0.25$.

The parameter $\bar{\chi}$ is measured by fitting the expected rate of like-sign dileptons $\mathcal{F}^{\rm ls}$, to the numbers of like-sign $n^{\rm ls}$ and opposite-sign $n^{\rm os}$ dilepton events found in the data:

$$-\ln\mathcal{L}_{\bar{\chi}^{\rm eff}} = -n^{\rm ls}\ln(\mathcal{F}^{\rm ls}) - n^{\rm os}\ln(1-\mathcal{F}^{\rm ls})\ . \tag{3}$$

As the statistical significance of the $\bar{\chi}$ measurement depends primarily upon the separation of the $b \to \ell$ and $b \to c \to \ell$ processes, a cut on $N_{\rm bl}$ is used. The contribution to $\mathcal{F}^{\rm ls}$ from the different processes is given in Table 1 for a cut $N_{\rm bl} > 0.5$.

A correction factor must be applied to $b \to c \to \ell$ decays to take into account differences in charged and neutral B mesons decays. These arise as neutral B mesons decay more frequently into a D^+, which has a higher semileptonic branching ratio than the D^0. The correction factor is determined from Monte Carlo. Fig. 8(a) and (b) display the results obtained for a set of different $N_{\rm bl}$ cuts, showing no significant trend. Fig. 8(c) shows the dependence of the correction factor upon the $N_{\rm bl}$ cut. The minimum total uncertainty is obtained for $N_{\rm bl} > 0.5$, which leaves 43,002 dilepton events. This gives

$$\bar{\chi} = 0.1196 \pm 0.0049\ (\text{stat.})\ ^{+0.0043}_{-0.0050}\ (\text{syst.}).$$

The breakdown of the systematic uncertainties is shown in Table 2.

Table 1: Contributions to the like-sign fraction from the different channels, along with their relative abundances (for events satisfying $N_{\rm uds} < 0.25$ and $N_{\rm bl} > 0.5$). Prompt leptons are denoted right and wrong sign depending on whether they preserve or not the charge of the parent quark (after any mixing has occurred). Background lepton candidates which can retain some information about the charge of the parent quark are denoted "bkg". Any pair in which one candidate originates from a charge-symmetric source is denoted as "symmetric", irrespective of the parent quark flavour. The probability $P_{\rm b}$ that a lepton of type "bkg" in b events has the same charge as the primary b quark is given by $P_{\rm b} = (1-\bar{\chi})\eta_{\rm b} + \bar{\chi}(1-\eta_{\rm b})$.

Flavour	Source	Fraction	Like-sign contribution
b	rs - rs	0.841	$2\bar{\chi}(1-\bar{\chi})$
	rs - ws	0.089	$\bar{\chi}^2 + (1-\bar{\chi})^2$
	ws - ws	0.002	$2\bar{\chi}(1-\bar{\chi})$
	rs - bkg	0.018	$\bar{\chi}P_{\rm b} + (1-\bar{\chi})(1-P_{\rm b})$
	ws - bkg	0.001	$\bar{\chi}(1-P_{\rm b}) + (1-\bar{\chi})P_{\rm b}$
	bkg - bkg	< 0.001	$2P_{\rm b}(1-P_{\rm b})$
c	rs - rs	0.009	0
	rs - bkg	0.001	$1-\eta_{\rm c}$
	bkg - bkg	< 0.001	$2\eta_{\rm c}(1-\eta_{\rm c})$
uds	bkg - bkg	0.002	$2\eta_{\rm uds}(1-\eta_{\rm uds})$
any	symmetric	0.037	0.5

7 Systematic uncertainties

The systematic uncertainties evaluated in the simultaneous b and c asymmetry measurement are reported in Table 2. The main effects are discussed below.

7.1 Semileptonic branching ratios

The semileptonic branching ratios BR(b $\to \ell$), BR(b $\to$ c $\to \ell$) and BR(c $\to \ell$) are important input parameters for the evaluation of the fractions $F_{\rm process}$. The values used are taken from the fit to the LEP and SLD results [17] excluding measurements of the heavy flavour asymmetries [18]:

$$\begin{aligned} {\rm BR(b} \to \ell) &= 0.1065 \pm 0.0023, \\ {\rm BR(b} \to {\rm c} \to \ell) &= 0.0804 \pm 0.0019, \\ {\rm BR(c} \to \ell) &= 0.0973 \pm 0.0033. \end{aligned}$$

In addition the following branching ratio values are used:

$$\begin{aligned} {\rm BR(b} \to \bar{\rm c} \to \ell) &= 0.0162 \pm 0.0044 \text{ [17]}, \\ {\rm BR(b} \to \tau \to \ell) &= 0.00419 \pm 0.00055 \text{ [17]}, \\ {\rm BR(b} \to {\rm u}\ell\nu) &= 0.0171 \pm 0.0053 \text{ [18]}, \\ {\rm BR(b} \to {\rm J}/\psi\ (\psi') \to \ell\ell) &= 0.00072 \pm 0.00006 \text{ [17]}. \end{aligned}$$

The branching ratio values are varied within their uncertainties to estimate the related systematic errors.

7.2 Modelling of semileptonic decays

The primary lepton energy in the rest frame of the weakly decaying b hadron in simulated events is reweighted to reproduce the spectra given by the ACCMM, ISGW and ISGW** models [16] tuned to CLEO data [19]. The ACCMM model is used for the result; the shifts observed with the

Table 2: Full list of systematic uncertainties. Numbers are given in units of 10^{-5}.

Error sources	$\Delta(A_{FB}^{b})$	$\Delta(A_{FB}^{c})$	$\Delta(\bar{\chi})$
BR($b \to \ell$)	∓ 18	± 53	± 92
BR($b \to c \to \ell$)	∓ 4	∓ 28	∓ 86
BR($c \to \ell$)	± 17	∓ 145	± 10
BR($b \to \bar{c} \to \ell$)	± 22	± 103	± 9
BR($b \to \tau \to \ell$)	± 5	∓ 23	± 6
BR($b \to u$)	± 2	± 3	± 7
Total BR	± 34	± 189	± 127
Electron ID	∓ 1	∓ 4	± 6
Muon ID	negl.	∓ 11	negl.
γ conversions	± 2	± 14	∓ 2
Electron bkg	± 2	± 20	∓ 2
Muon bkg ($K, \pi \to \mu$)	negl.	negl.	negl.
Muon bkg (misid. K, π)	± 4	± 65	∓ 29
Muon ID (low p)	∓ 1	negl.	∓ 29
IP smearing	∓ 6	∓ 53	–
Secondary VTX smearing	∓ 13	∓ 4	–
Detector Systematics	± 15	± 88	± 41
$b \to \ell$ model	$^{+21}_{-1}$	$^{-80}_{+96}$	$^{+103}_{-175}$
$c \to \ell$ model	$^{+53}_{-41}$	$^{-87}_{+47}$	$^{-250}_{+224}$
$b \to D$ model	$^{-2}_{+1}$	$^{-19}_{+16}$	$^{-283}_{+227}$
BR($b \to D^{**}$)	± 58	± 164	∓ 105
$p_\perp$ charm	negl.	∓ 23	± 3
b fragmentation	negl.	∓ 30	∓ 58
c fragmentation	± 45	∓ 46	± 11
Total modelling	$^{+93}_{-84}$	$^{+205}_{-212}$	$^{+356}_{-433}$
Bkg charge correlation	± 1	∓ 62	negl.
A_{FB}^{s}	negl.	± 26	–
A_{FB}^{d}	± 1	± 23	–
A_{FB}^{u}	negl.	± 8	–
Total bkg asymmetries	± 2	± 72	negl.
R_b	∓ 2	± 6	negl.
R_c	± 11	∓ 75	± 2
Gluon splitting ($b\bar{b}$)	∓ 2	± 1	∓ 36
Gluon splitting ($c\bar{c}$)	∓ 1	± 14	∓ 29
b hadron lifetimes	± 2	∓ 12	± 4
b hadron fractions	∓ 4	± 31	± 48
b multiplicity	∓ 10	∓ 5	negl.
c hadron lifetimes	∓ 9	± 68	∓ 2
c hadron fractions	± 21	∓ 81	± 9
K^0 production in c decays	∓ 13	± 19	∓ 6
c hadron topological rates	± 10	± 95	± 4
Total B and D physics	± 32	± 166	± 68
mixing	± 128	± 12	–
$b \to c \to \ell$ mixing correction	∓ 34	∓ 112	∓ 180
Total Mixing	± 132	± 113	± 180
TOTAL	± 169	± 369	$^{+431}_{-496}$

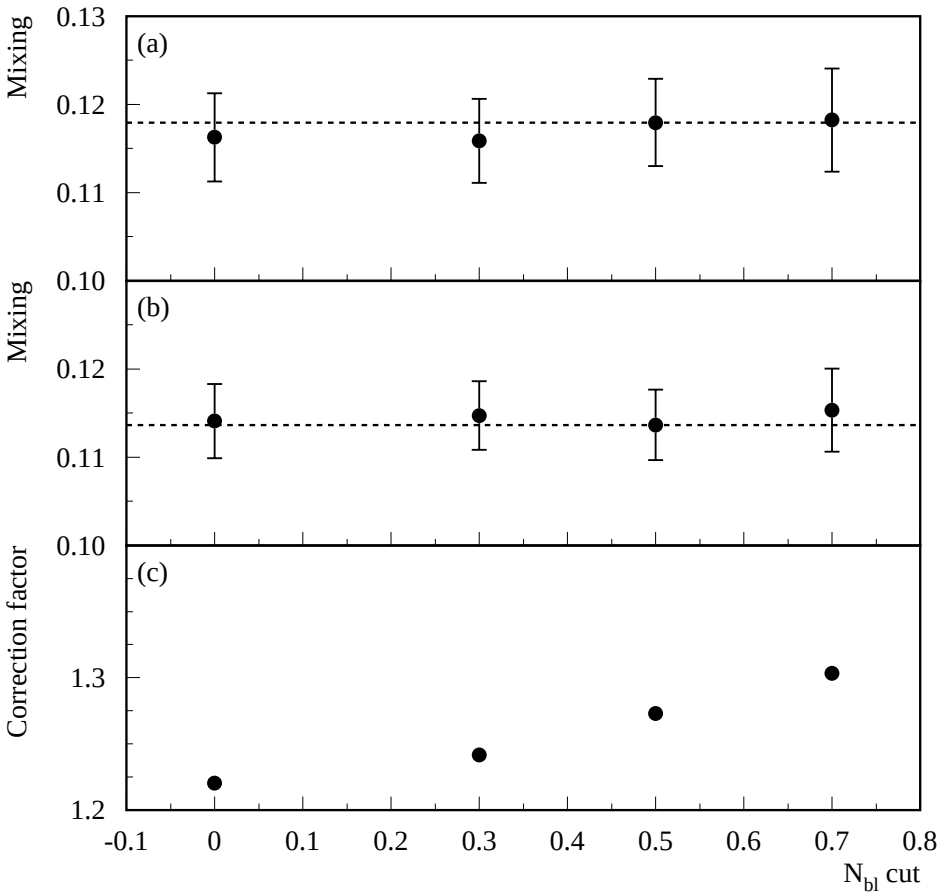

Figure 8: Stability of the mixing result as a function of the $N_{\rm bl}$ cut for (a) the data, (b) the simulation. The error bars represent the statistical errors. The cut $N_{\rm bl} > 0.5$ minimizes the total error. Plot (c) displays the dependence of the correction factor applied to the $b \to c \to \ell$ component upon the $N_{\rm bl}$ cut.

ISGW and ISGW** models are taken as systematic uncertainty. For $c \to \ell$ decays the ACCMM model is used, with the model parameters determined from MARK III [20] and DELCO [21] data. The lepton energy spectrum for cascade $b \to c \to \ell$ decays is obtained as the convolution of the $b \to D$ spectrum measured by CLEO [22] with the $c \to \ell$ spectrum.

The discriminating quantity $N_{\rm bl}$ is also sensitive to the fraction of D^{**} in B decays through the jet properties, which reflect the dynamics of the b hadron decay. These effects are globally accounted for by varying the relative production of D^{**} states in the Monte Carlo simulation, according to $f_{D^{**}} = 20 \pm 10\%$.

The clustering cut in the jet definition (Section 2) has been tuned so that the lepton transverse momentum provides an optimal separation between the $b \to \ell$ and $b \to c \to \ell$ decays. In the case of charm semileptonic decays, the jet contains typically many fragmentation particles, and therefore the $p_\perp$ distribution of $c \to \ell$ decays in the simulation is affected by the modelling of that component, as discussed in [1]. This has been studied using $D^{*+} \to D^0\pi^+$ decays followed by $D^0 \to K^-\ell^+\nu$. The ratio of the spectra measured in data and simulation provides correction factors, which typically differ from unity by less than 20%. They are used to reweight simulated events and their statistical errors are used to estimate the systematic uncertainty.

The fragmentation of b and c quarks into hadrons follows the model of Peterson *et al.* [23]. The free parameters of the model are tuned to reproduce the measured values of the average

heavy hadron energy [17]; they are varied according to the uncertainty on the experimental measurements to estimate the related systematic uncertainty.

7.3 Lepton identification and misidentification of hadrons

The assignment of the uncertainties related to lepton identification follows the procedure defined in [7, 8]. Correction factors for lepton efficiency and misidentification rates are estimated from the data and applied to simulated events. Electron and muon identification efficiencies are measured with an uncertainty of about 2%. The uncertainty on the rate of photon conversions and non-prompt muons from K and π decays is estimated to be about 10%. A 20% uncertainty is assigned to the rate of K and π misidentified as muons.

7.4 Background asymmetry

The forward-backward asymmetry in $Z \to u\bar{u}$, $Z \to d\bar{d}$ and $Z \to s\bar{s}$ events is taken from the Standard Model expectation. The study of the background component that retains some information of the original quark charge follows the procedure described in [1]. The systematic error is estimated by assigning a 20% uncertainty to this effect in the simulation.

7.5 b and c physics

The Monte Carlo is reweighted to reproduce the world average values of the partial widths R_b and R_c, of the b hadron and c hadron production rates, their lifetimes and the average charged track multiplicity in b and c events [17, 24]. The systematic errors related to these quantities are estimated by varying them within their uncertainties. In particular, the charged track multiplicity in c events is corrected by reweighting the c hadron topological decay modes to the values given in [17].

The production rates of c and b quark pairs originating from radiated gluons are taken to be [17] $P(g \to c\bar{c}) = (2.96 \pm 0.38)\%$ and $P(g \to b\bar{b}) = (0.254 \pm 0.051)\%$.

7.6 Mixing

As explained in Section 5, the probability that a neutral B meson has oscillated is determined in each bin of the analysis from simulated events, reweighted to reproduce the measured value of the average time-integrated mixing rate. A systematic uncertainty on the asymmetry is assigned by varying the mixing parameter by its statistical uncertainty. For each systematic effect common to the mixing and asymmetry measurements, the correlation is taken into account in the estimate of the uncertainty on the asymmetry. A conservative estimate of the systematic error due to the correction factor applied for $b \to c \to \ell$ decays is obtained by setting it to unity.

7.7 Tracking

Differences in the tracking performance between data and simulation result in some discrepancies in the distribution of P_E and $\Delta\chi^2_V$. To improve the agreement, a smearing is applied to the measured track impact parameters and reconstructed secondary vertices in the simulation as described in [25, 2]. The full change resulting from each smearing procedure is assigned as a sytematic uncertainty.

7.8 Monte Carlo statistics

In order to evaluate the uncertainty due to the finite statistics of the simulated data sample, the Monte Carlo events are split into 8 subsamples. The fit to the data is performed using each subsample to estimate F, $\bar{\chi}$, η (see Section 5). The spread between the results of the 8 fits is found to be negligible.

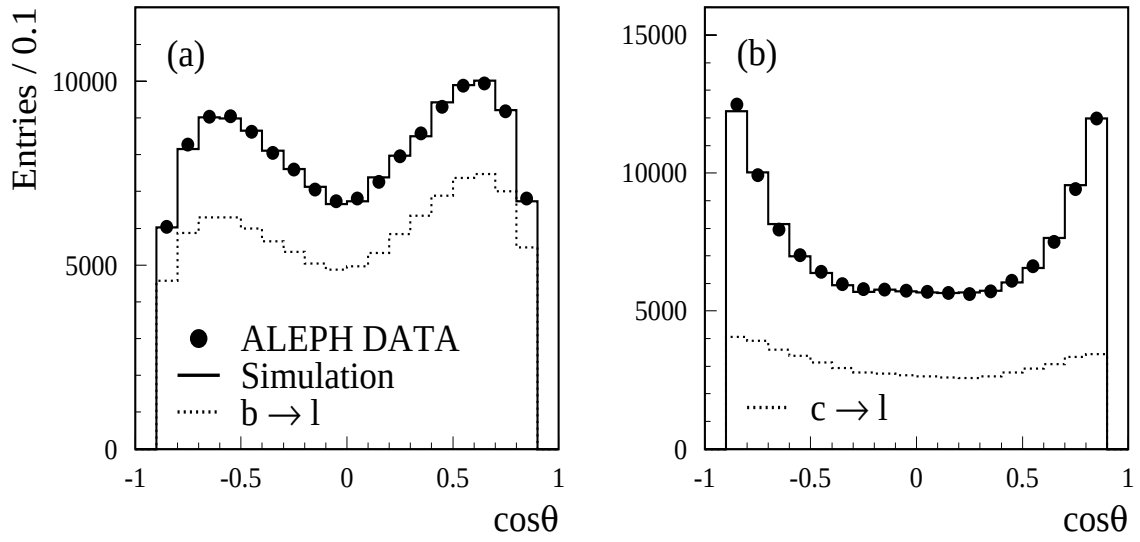

Figure 9: Observed angular distribution in (a) a b-enhanced region, (b) a c-enhanced region. The full histogram shows the expected raw angular distribution in the simulation reweighted according to the result of the fit. The dashed histogram shows the angular distribution of (a) the $b \to \ell$ component, (b) the $c \to \ell$ component.

Table 3: A^b_{FB} and A^c_{FB} measurements at each off-peak center-of-mass energy with statistical and systematic uncertainties.

$\sqrt{s}$ (GeV)	A^b_{FB}	A^c_{FB}
88.38	$-0.131 \pm 0.135 \pm 0.010$	$-0.124 \pm 0.159 \pm 0.020$
89.38	$0.055 \pm 0.019 \pm 0.001$	$-0.023 \pm 0.026 \pm 0.002$
90.21	$-0.004 \pm 0.067 \pm 0.008$	$-0.003 \pm 0.083 \pm 0.006$
92.05	$0.111 \pm 0.064 \pm 0.005$	$0.106 \pm 0.077 \pm 0.007$
92.94	$0.104 \pm 0.015 \pm 0.003$	$0.119 \pm 0.021 \pm 0.006$
93.90	$0.138 \pm 0.093 \pm 0.011$	$0.121 \pm 0.110 \pm 0.010$

8 The fit results and the extraction of $\sin^2\theta^{\rm eff}_{\rm W}$

Fig. 9 displays the observed angular distributions at peak energy in b-enhanced and c-enhanced regions, illustrating the asymmetries in $Z \to b\bar{b}$ and $Z \to c\bar{c}$ events. The drop in acceptance at low angles for the b-enhanced sample (a) is due to the fact that the b quark selection depends primarily on the lifetime measurements based upon the VDET information. An asymmetry in the angular distribution of the events in the c-enriched sample is seen, in spite of the large contribution at low angles of the symmetric background component.

The b and c asymmetries at peak energy are measured to be

$$\begin{aligned} A^b_{FB}\ (\sqrt{s} = 91.21\ \text{GeV}) &= 0.0952 \pm 0.0041\ (\text{stat.}) \pm 0.0017\ (\text{syst.}), \\ A^c_{FB}\ (\sqrt{s} = 91.21\ \text{GeV}) &= 0.0645 \pm 0.0057\ (\text{stat.}) \pm 0.0037\ (\text{syst.}). \end{aligned}$$

The statistical correlation between these two measurements is found to be 14%.

The results for the statistics collected at the other six centre-of-mass energies are reported in Table 3 and displayed in Fig. 10 together with the peak values.

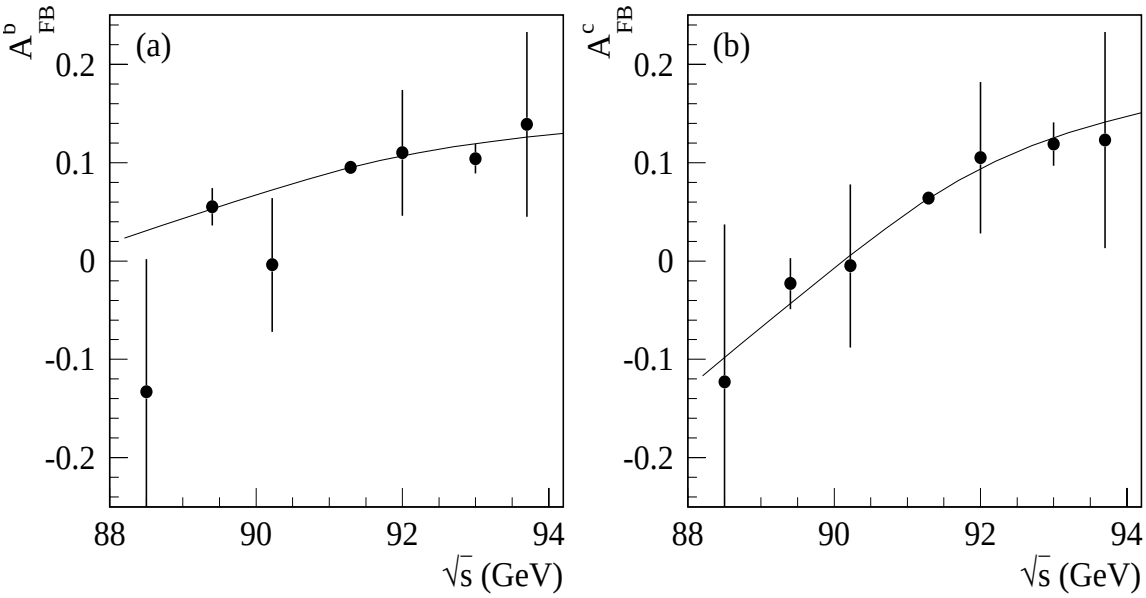

Figure 10: (a)A^b_{FB} and (b)A^c_{FB} measurements as a function of the centre-of-mass energy. The curve is the Standard Model expectation fitted to the measured values of the asymmetries.

Gluon radiation distorts the quark angular distribution, compared to the pure electroweak process. Analytic calculations that predict these effects for the asymmetries are reviewed in [17, 26] and taken as a bare correction to the measurements. However, the sensitivity of a measurement to these effects depends upon the event selection and the analysis technique, and an experimental scaling factor $s^{\mathrm{QCD}}_{\mathrm{b,c}}$ to be applied to the bare correction needs to be evaluated case by case. Therefore, the measurements are repeated on high statistics $\mathrm{Z} \to \mathrm{b\bar{b}}$ and $\mathrm{Z} \to \mathrm{c\bar{c}}$ Monte Carlo samples and the results are compared with the same events at generator level, yielding the values of the experimental scaling factors $s^{\mathrm{QCD}}_{\mathrm{b}} = 0.91 \pm 0.23$ and $s^{\mathrm{QCD}}_{\mathrm{c}} = 0.00^{+0.49}_{-0.00}$. The correction factors to the observable asymmetry are therefore 1.0269 ± 0.0068 and $1.000^{+0.018}_{-0.000}$, respectively for the b and c asymmetries.

In order to interpret the results in the framework of the Standard Model, they are extrapolated to $\mathrm{M_Z} = 91.1874$ GeV/c^2 and the QED and Z-γ interference corrections are applied according to [17].

The asymmetry measurements performed at peak and off-peak energies result in the following measurement of the pole asymmetries, or equivalently, of the electroweak mixing angle:

$$\begin{aligned} \mathrm{A^{0,b}_{FB}} &= 0.0998 \pm 0.0040\ (\mathrm{stat.}) \pm 0.0017\ (\mathrm{syst.}), \\ \mathrm{A^{0,c}_{FB}} &= 0.0732 \pm 0.0053\ (\mathrm{stat.}) \pm 0.0037\ (\mathrm{syst.}), \\ \sin^2\theta^{\mathrm{eff}}_{\mathrm{W}} &= 0.23203 \pm 0.00073. \end{aligned}$$

9 Checks

Various checks of the consistency of the method and the stability of the results are discussed in the following.

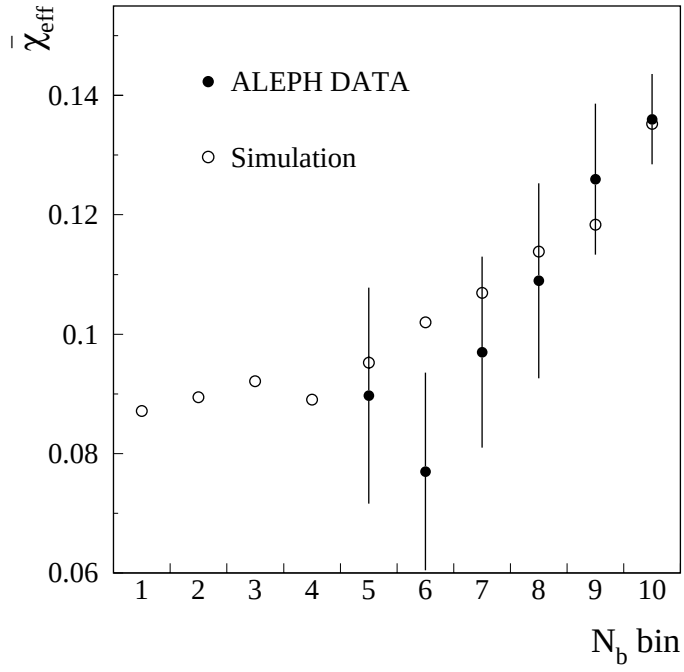

Figure 11: Distribution of the measured value of the effective mixing in bins of $N_{\rm b}$. Open circles display the Monte Carlo expectation.

9.1 Results on the electron and muon samples

The heavy quark asymmetries are measured separately on the samples containing electron or muon candidates at peak energy. Consistent results are obtained as shown in Table 4. In the fit to the global sample, the two lepton species are not distinguished and the average sample composition is used. This fact explains the small difference between the average of the values reported in Table 4 and the result of the full fit.

Table 4: $A^{\rm b}_{\rm FB}$ and $A^{\rm c}_{\rm FB}$ at peak energy with the electron and muon candidate samples fitted separately.

	electrons	muons
$A^{\rm b}_{\rm FB}$	$0.0956 \pm 0.0060 \pm 0.0018$	$0.0944 \pm 0.0055 \pm 0.0017$
$A^{\rm c}_{\rm FB}$	$0.0589 \pm 0.0082 \pm 0.0033$	$0.0694 \pm 0.0078 \pm 0.0043$

9.2 Measurement with a simultaneous fit of the mixing

As discussed in Section 5, the use of the lifetime information introduces a dependence of the effective time-integrated mixing upon $N_{\rm b}$. The effective mixing parameter can be measured simultaneously with the asymmetries in the high purity region $N_{\rm b} > 0.65$, while the prediction of the simulation after reweighting is still taken for the remaining bins.

Fig. 11 shows a comparison of the effective mixing measurements and the Monte Carlo expectation.

The simultaneous fit yields, on peak energy data:

$$\begin{aligned} A^{\rm b}_{\rm FB} &= 0.0938 \pm 0.0042 \text{ (stat.)} \pm 0.0012 \text{ (syst.)}, \\ A^{\rm c}_{\rm FB} &= 0.0644 \pm 0.0057 \text{ (stat.)} \pm 0.0037 \text{ (syst.)}, \end{aligned}$$

in good agreement with the results obtained using the prediction of the reweighted Monte Carlo. For the b asymmetry, the uncorrelated statistical uncertainty between the two methods is estimated to be about 0.0012. Due to lack of statistics, this method cannot be applied to the off-peak center-of-mass energy samples.

9.3 $A^b_{FB}(A^c_{FB})$ measurement in a high b(c)-purity sample

The fit to the asymmetries is repeated restricting the analysis to high purity subsamples, in order to check possible systematic effects related to the modelling of the background in the low-purity regions. A fit for the b asymmetry is performed in the regions defined by $N_b > 0.9$ and $N_{bl} > 0.5$, respectively, while the c asymmetry is fixed to its measured value:

$$\begin{aligned} \text{b-enhanced region} \qquad & \delta A^b_{FB} = -0.0009 \ , \\ (b \to \ell)\text{-enhanced region} \qquad & \delta A^b_{FB} = +0.0011 \ , \end{aligned}$$

where δA^b_{FB} is the difference between the value measured in the restricted region and the result of the full fit. Both results are in agreement with the reference value within the uncorrelated statistical uncertainty of 0.0015.

A similar check is performed for the c asymmetry by restricting the fit to the region $N_b < 0.5$ and $N_{uds} < 0.5$, yielding $\delta A^c_{FB} = -0.0044$. Satisfactory agreement with the reference analysis is achieved, as the uncorrelated statistical uncertainty is 0.0036.

9.4 Semileptonic b and c branching ratios and fake rates

The discrimination between the $b \to \ell$ and $b \to c \to \ell$ processes is good enough to allow a simultaneous measurement of their branching ratios with the heavy flavour asymmetries. If that resulted in significantly different values of A^b_{FB} or A^c_{FB}, it would indicate that systematic uncertainties related to the primary lepton modelling are not under control. The first column in Table 5 shows the results of the fit; the A^b_{FB} and A^c_{FB} values so obtained are in agreement with the reference measurements. In addition, the semileptonic b branching ratios are in good agreement with the present LEP averages, used as input to the asymmetry measurement.

Table 5: Summary of the checks performed with a simultaneous measurement of: 1) the semileptonic branching ratios BR($b \to \ell$) and BR($b \to c \to \ell$), 2) the semileptonic branching ratio BR($c \to \ell$), 3) the rate of charge asymmetric background in b and c events, $R^{bkg}_{b,c}$, and 4) the rate of nonprompt and fake leptons in light quark events, R^{bkg}_{uds}. Results in the upper table are expressed in terms of the absolute variation of A^b_{FB} (A^c_{FB}), denoted δA^b_{FB} (δA^c_{FB}). The lower table displays for checks 1) and 2) the comparison of the input and fitted values for BR($b \to \ell$), BR($b \to c \to \ell$) and BR($c \to \ell$).

Checks	1)	2)	3)	4)
δA^b_{FB}	$+0.0006$	$+0.0004$	$+0.0001$	< 0.0001
δA^c_{FB}	$+0.0009$	$+0.0021$	-0.0004	-0.0002

Checks	1) BR($b \to \ell$)	1) BR($b \to c \to \ell$)	2) BR($c \to \ell$)
Input value	0.1065 ± 0.0023	0.0804 ± 0.0019	0.0973 ± 0.0033
Fitted value (stat. error only)	0.1088 ± 0.0004	0.0807 ± 0.0008	0.0935 ± 0.0005

Similar exercises are performed by fitting simultaneously with the heavy flavour asymmetries the charm semileptonic branching ratio, the ratio of charge asymmetric background in b and c events in data and Monte Carlo, denoted $R^{bkg}_{b,c}$, and the ratio of nonprompt and fake leptons in Z decays to light quarks in data and Monte Carlo, R^{bkg}_{uds}. These tests are mainly intended to check for systematic effects related to the estimate of the charge symmetric and

asymmetric background rates. As in the previous case, the changes in the asymmetry values are remarkably small and fully contained in the assigned systematic uncertainty. The results are reported in Table 5. The fake rate ratios are measured to be $R_{\mathrm{b,c}}^{\mathrm{bkg}} = 0.94 \pm 0.01$ (stat.) and $R_{\mathrm{uds}}^{\mathrm{bkg}} = 0.997 \pm 0.004$ (stat.), the difference from unity being well below the associated systematic uncertainty. All these checks justify the description of the lepton candidate sample in the simulation. The stability of the asymmetry results provides confidence in the systematic error estimates.

10 Combination of ALEPH measurements

ALEPH published a measurement of the c asymmetry using reconstructed D mesons [3] and a measurement of the b asymmetry using inclusive b hadron decays [2]. These measurements are averaged with the one presented in this paper following the procedure described in [16]. The two b asymmetry analyses use partially overlapping samples and the average hemisphere charge flow [2] is better defined in the presence of a lepton from semileptonic b-hadron decay, even if the lepton properties are not explicitly used. In order to determine the statistical correlation between the lepton and inclusive measurements, the data recorded at peak energy are split into approximately 600 samples and the analyses are performed simultaneously on each sample. The statistical correlation parameter is measured to be (0.264 ± 0.039). Systematic uncertainties in both measurements are treated as uncorrelated.

The pole asymmetry for b and c quarks, derived from the combination of the measurements, are found to be

$$\begin{aligned} \mathrm{A}_{\mathrm{FB}}^{0,\mathrm{b}} &= 0.1011 \pm 0.0026, \\ \mathrm{A}_{\mathrm{FB}}^{0,\mathrm{c}} &= 0.0720 \pm 0.0052. \end{aligned}$$

The χ^2 of the combination is 7.7 for 18 degrees of freedom.

The final ALEPH result on the electroweak mixing angle from heavy flavour asymmetries is

$$\sin^2\theta_{\mathrm{W}}^{\mathrm{eff}} = 0.23188 \pm 0.00046.$$

11 Conclusion

In a data sample of about 3.9 million hadronic Z decays recorded with the ALEPH detector at LEP in the years 1991-1995, a simultaneous measurement of the b and c asymmetries and a measurement of the B^0–$\bar{\mathrm{B}}^0$ average mixing parameter are performed by means of leptons originating from the semileptonic decays of heavy flavour hadrons. The data are analysed as a function of the polar angle of the thrust axis in a space of discriminating variables aimed at separating lepton candidates according to the flavour and to the physics process from which they originate. The values of the pole asymmetries obtained by combining the b and c asymmetry measurements at the seven energy points, and unfolding QED and QCD effects, are

$$\begin{aligned} \mathrm{A}_{\mathrm{FB}}^{0,\mathrm{b}} &= 0.0998 \pm 0.0040 \text{ (stat.) } \pm 0.0017 \text{ (syst.)}, \\ \mathrm{A}_{\mathrm{FB}}^{0,\mathrm{c}} &= 0.0732 \pm 0.0053 \text{ (stat.) } \pm 0.0037 \text{ (syst.)}, \end{aligned}$$

in agreement with previous ALEPH and LEP measurements [1, 14, 27]. These measurements are the most precise among the analyses based upon the lepton tagging technique.

The main systematic uncertainty affecting the b asymmetry measurement is due to B^0–$\bar{\mathrm{B}}^0$ mixing while the c asymmetry systematic uncertainties are primarily due to the modelling of B and D physics in the simulation. The average integrated mixing parameter is measured from a sample of events containing two lepton candidates, obtaining

$$\bar{\chi} = 0.1196 \pm 0.0049 \text{ (stat.)} \, {}^{+0.0043}_{-0.0050} \text{ (syst.)}.$$

The combination of all the ALEPH heavy flavour asymmetry measurements yields

$$\sin^2\theta^{\rm eff}_{\rm W} = 0.23188 \pm 0.00046.$$

This determination of the electroweak mixing angle is consistent with the values derived from the ALEPH measurements of the τ polarization [28] and lepton asymmetries [6].

Acknowledgements

We wish to thank our colleagues in the CERN accelerator divisions for the successful operation of LEP. We are indebted to the engineers and technicians in all our institutions for their contributions to the excellent performance of ALEPH. Those of us from non-member countries thank CERN for its hospitality.

References

[1] ALEPH Collaboration, "Measurement of the b forward-backward asymmetry and mixing using high $p_\perp$ leptons", Phys. Lett. **B384** (1996) 414.

[2] ALEPH Collaboration, "Measurement of A^b_{FB} using inclusive b-hadron decays", CERN-EP/2001-047, to be published in Eur. Phys. J. .

[3] ALEPH Collaboration, "The Forward-Backward Asymmetry for Charm Quarks at the Z", Phys. Lett. **B434** (1998) 415.

[4] ALEPH Collaboration, "Performance of the ALEPH detector at LEP", Nucl. Instr. Methods **A360** (1995) 481.

[5] ALEPH Collaboration, "ALEPH: a detector for electron-positron annihilations at LEP", Nucl. Instr. Methods **A294** (1990) 121.

[6] ALEPH Collaboration, "Measurement of the Z resonance parameters at LEP", Eur. Phys. J. **C** 14 (2000) 1.

[7] ALEPH Collaboration, "Heavy quark tagging with leptons in the ALEPH detector", Nucl. Instr. Methods **A346** (1994) 461.

[8] ALEPH Collaboration, "Inclusive semileptonic branching ratios of b hadrons produced in Z decays", CERN-EP/2001-057, to be published in Eur. Phys. J. C.

[9] ALEPH Collaboration, "Investigation of inclusive CP asymmetries in B^0 Decays", Eur. Phys. J. **C** 20 (2001) 431-443.

[10] JADE Collaboration, "Experimental studies on multijet production in e^+e^- annihilations at PETRA energies", Z. Phys. **C33** (1986) 23.

[11] ALEPH Collaboration, "A precise measurement of $\Gamma_{Z\to b\bar{b}}/\Gamma_{Z\to had}$", Phys. Lett. **B313** (1993) 535.

[12] ALEPH Collaboration, "An investigation of B^0_d and B^0_s oscillation", Phys. Lett. **B322** (1994) 441.

[13] ALEPH Collaboration, "Measurement of the branching fraction for $D^0 \to K^-\pi^+$", Phys. Lett. **B403** (1997) 367.

[14] ALEPH Collaboration, "Heavy flavour production and decay with prompt leptons in the ALEPH detector", Z. Phys. **C62** (1994) 179.

[15] OPAL Collaboration, "Measurement of heavy quark forward-backward asymmetries and average $B^0-\bar{B}^0$ mixing using leptons in multihadronic events", Z. Phys. **C70** (1996) 357.

[16] LEP and SLD Collaborations, "Combining Heavy Flavour Electroweak Measurements at LEP", Nucl. Instr. Methods **A378** (1996) 101.

[17] The ALEPH, DELPHI, L3, OPAL Collaborations, the LEP Electroweak Working Group and the SLD Electroweak and Heavy Flavour Groups, "Precision Electroweak Measurements on the Z Resonance". Physics Report in preparation.

[18] F. Palla, "Semileptonic B decays and CKM elements at LEP", in Proceedings of the EPS International Conference on High Energy Physics, Budapest, 2001 (D. Horvath, P. Levai, A. Patkos, eds.), JHEP (http://jhep.sissa.it/) Proceedings Section, PrHEP-hep2001/077.

[19] CLEO Collaboration, "Measurements of semileptonic branching fractions of B mesons at the $\Upsilon(4S)$ resonance", Phys. Rev. **D45** (1992) 2212.

[20] MARK III Collaboration, "Direct measurement of charmed D^+ and D^0 semileptonic branching ratios", Phys. Rev. Lett. **54** (1985) 1976.

[21] DELCO Collaboration, "Semileptonic decays of the D meson", Phys. Rev. Lett. **43** (1979) 1073.

[22] CLEO Collaboration, "Inclusive and exclusive decays of B mesons to final states including charm and charmonium mesons", Phys. Rev. **D45** (1992) 21.

[23] C. Peterson *et al.*, "Scaling violations in inclusive e^+e^- annihilations spectra", Phys. Rev. **D27** (1983) 105.

[24] ALEPH, CDF, DELPHI, L3 and SLD Collaborations, "Combined results on b-hadron production rates, lifetimes, oscillations and semileptonic decays", CERN-EP/2001-050.

[25] ALEPH Collaboration, "A measurement of R_b using mutually exclusive tags", Phys. Lett. **B401** (1997) 150.

[26] D. Abbaneo *et al.*, "QCD corrections to the forward-backward asymmetries of c and b quarks at the Z pole", Eur. Phys. J. **C**4 (1998) 185.

[27] DELPHI Collaboration, "Measurement of the Forward-Backward Asymmetry of $e^+e^- \to Z \to Z \to b\bar{b}$ using prompt leptons and a lifetime tag", Z. Phys. **C65** (1995) 569;
L3 Collaboration, "Measurement of the $e^+e^- \to Z \to b\bar{b}$ Forward-Backward Asymmetry and the $B^0-\bar{B}^0$ Mixing Parameter Using Prompt Leptons", Phys. Lett. **B448** (1999) 152;
OPAL Collaboration, "Measurement of heavy quark forward-backward asymmetries and average $B^0-\bar{B}^0$ mixing using leptons in multihadronic events", Z. Phys. **C70** (1996) 357.

[28] ALEPH Collaboration, "Measurement of the τ polarisation at LEP1", Eur. Phys. J. **C** 20 (2001) 401.